# Oxygen Reduction and Oxygen Evolution on $SrTi_{1-x}Fe_xO_{3-y}$ (STFO) Perovskite Electrocatalysts

Brian E. Hayden* and Fiona K. Rogers

Chemistry, The University of Southampton, Highfield,

Southampton SO17 1BJ, UK

Keywords: Oxygen Reduction, Oxygen Evolution, Perovskite, Electrocatalysis

Compositionally graduated thin films of a $SrTi_{1-x}Fe_xO_{3-y}$ (STFO) perovskite electrocatalysts were successfully prepared by High Throughput Physical Vapour Deposition (HT-PVD) using evaporative sources. X-ray diffraction confirmed a continuous solid solution of the cubic perovskite structure with an increase in the lattice parameter with increasing x from 0.392 ± 0.001 nm for $SrTiO_3$ to 0.386 ± 0.001 nm for $SrFeO_3$. A Raman mode corresponding to an O-stretching vibration was observed which is disallowed by symmetry in the cubic structure suggests a localised lattice distortion. The perovskites exhibited poor conductivity for low values of x ($\rho < 7 \times 10^{-8}$ S cm$^{-1}$) but conductivity increased with increasing Fe content before reaching a plateau at $\rho = 0.041$ S cm$^{-1}$ for x > 0.75. Increasing electrocatalytic activity towards the oxygen evolution reaction (OER) with increasing Fe content was observed, characterised by a 100 μA onset potential varying monotonically from $1.52V_{RHE}$ (x = 0.2) to $1.40V_{RHE}$ (x = 0.85). The high OER activity was however found to correlate with low electrode stability, consistent with the participation of lattice oxygen in the OER mechanism. The latter was evidenced by the redox electrochemistry associated with reversible oxygen intercalation. $SrTi_{0.5}Fe_{0.5}O_{3-y}$ exhibited the optimal composition with good OER activity and electrode stability. Low electrocatalytic activity towards the oxygen reduction reaction (ORR) was observed for all oxygen stoichiometric compositions. The ORR did not occur until after reduction of the films suggesting that surface reduction is required for the creation of the active surface sites. ORR activity on the oxygen sub-stoichiometric perovskites showed the opposite trend with compositional variation to OER activity on the oxygen stoichiometric perovskites.

* Corresponding Author

## 1. Introduction

Transition metal oxides provide several advantages over metal surfaces for catalysis of the ORR as well as the OER. Firstly, metal oxides are the thermodynamically stable state of most metals at potentials required for the ORR and OER. Additionally, oxide surfaces have redox and acid/base functionality which aids electron transfer and therefore electrocatalysis. Finally, metal oxides are much cheaper and more abundant than noble metal catalysts. Whilst many oxides have shown promise as ORR/OER catalysts due to their low over-potentials, which are comparable to Pt catalysts, the reported current densities have been low since catalysis is kinetically limited on the oxide surface by poor electron transport [1]. The development of better oxide-based electrocatalysts is therefore linked to the reduction in the band gap of oxide materials and the concomitant improvement of electronic conductivity. One approach to the development of electronically conducting oxide electrocatalysts focuses on oxides with crystal structures containing multiple metal ions such as those with the spinel structure, $A[B_2]O_4$, and the perovskite structure, $ABO_3$, which have also been investigated for their OER and ORR activity [2-10]. These materials can support multiple metal cations at the A and B sites as well as oxygen vacancies which encourage redox activity. This has the effect of improving the mobility of electrons and oxide ions through the structure and as such improves the electronic and ionic conductivity. The significance of the introduction of redox activity into ORR/OER electrocatalysts extends beyond the improvement of electronic conductivity and there is evidence to support the involvement of redox reactions in the ORR and OER mechanisms. One example of this is in manganese oxides which have shown promise as ORR electrocatalysts in alkaline media [11-14]. Cao *et al.* [11] studied various different $MnO_2$ catalysts and identified a link between the $Mn^{3+}/Mn^{4+}$ redox couple and ORR activity. They used voltammetry to observe that oxygen reduction current increased with increasing electro-reduction of the film and proposed that the ORR mechanism required the presence of $Mn^{3+}$ which is then able to donate an electron to oxygen resulting in the oxidation of $Mn^{3+}$ to $Mn^{4+}$.

We have applied a combinatorial synthetic methodology to produce compositional gradient thin films of $SrTi_{1-x}Fe_xO_{3-y}$ (STFO). $SrTiO_3$ (STO) is an insulator with a band gap of 3.2 eV [15]. The conductivity can be improved by the substitution of Ti by Fe, and STFO adopts the cubic perovskite structure across the solid solution from $SrTiO_3$ (STO) to $SrFeO_{3-y}$ (SFO) [16-18]. Importantly, Fe was selected in this investigation because the $Fe^{4+}$ ion adopts a high spin $d^4$ electronic structure which has been linked to high OER [3] and ORR [19] activity. STFO materials also have interesting redox properties since Fe is also able to adopt the $Fe^{3+}$ oxidation state which creates oxygen vacancies in the lattice. The extent of oxygen deficiency in the lattice is represented above by the value of y.

## 2. Experimental

### 2.1 Catalyst Synthesis

Compositional gradient thin film samples were deposited by High Throughput (evaporative) Physical Vapour Deposition (HT-PVD) [20]. This approach has previously been employed to prepare complex oxides, including those with the perovskite structure, by including, together with Knudson cells or e-gun sources, a plasma atom source to provide oxygen atoms [21-24]. Elements are deposited simultaneously using multiple off-axis sources, each source independently shadowed by a partial "wedge" shutter which controls the flux distribution across the substrate. Simultaneous mixing of the elements provides a low kinetic energy to solid state oxide formation providing a low temperature route to amorphous and crystalline stoichiometric oxides. The position of the wedge shutters determine the compositional region being deposited at the substrate [20].

The HT-PVD deposition chamber has a base-pressure of ca. 1 x $10^{-9}$ mbar with pumping via a cryo-pump alongside a turbo-molecular pump backed by an oil-free rotary pump. Oxygen was introduced into the chamber either in molecular form, or as atoms generated using a plasma atom source (Oxford Applied Research). Ti (pellets, 99.995%, Testbourne) and Fe (granules, 99.95%, Testbourne) were evaporated from electron-beam evaporators. The Sr (pieces, 99.9%, Testbourne) evaporation was achieved from a Knudsen cell. The substrate was heated to 650 °C in order to induce direct crystallisation of the thin films during synthesis.

The thin films were deposited onto 35 x 35 mm substrates of Si and SiN for characterisation. For electrochemical measurements, the films were deposited onto the 1$mm^2$ pads of an electrochemical screening chip consisting of a 10x10 array of ITO electrode pads with tracks connecting to edge electrical contacts, in a geometry identical to that used (and described) elsewhere [25]. A layer of $SiO_2$ was used to prevent contact of the ITO tracks with the electrolyte. A contact deposition (shadow) mask was used to limit film deposition to the area of the electrode pads: The windows of the mask were slightly larger than the electrode pads to ensure that all the ITO was covered in the deposition.

### 2.2 Perovskite Characterisation

The composition of the films was determined using an EDX micro-analyser (Oxford Inca 300) coupled with a scanning electron microscope (Jeol, JSM 5910) for surface imaging so that EDX measurements could be performed at specific known points on the sample corresponding to the 100 discrete electrodes of the electrochemical array. The error in the

compositions obtained from EDX measurements was estimated to be ca. ± 2 at.%, corresponding to an error in x (where x = Fe/(Ti+Fe)) of ± 0.4%. The compositional region covered in this work were synthesised in two separate electrochemical arrays, with 100 electrocatalysts on each array (Supplementary Information S.1). A P16 Stylus Profiler (KLA Tencor) was used to measure the thickness of the thin film catalysts, which were ca. 300nm in the region of the perovskite compositional tie-line.

XRD data was obtained using a Bruker D8 instrument incorporating a C2 detector. Raman spectra were measured using a Raman microscope (Horiba Xplora) encorporating a 532 nm laser. The conductivity of the STFO thin films was calculated from the sheet resistance, measured with a Model 280DI Four-Point Probe Mapping System (Four Dimensions) and a Van der Pauw probe. The thin film perovskite was synthesised on a Si/SiN wafer for these measurements.

### 2.3 Electrochemistry

The high-throughput electrochemical measurements were made using a three-compartment electrochemical cell specifically designed to accommodate the high-throughput electrochemical array [26]. A printed circuit board was used to connect the external contact pads of the array to a 100-channel potentiostat via two 50-way cables. A Pt mesh was used as a counter electrode inside a compartment separated from the main cell by a glass sinter. A Hg/HgO reference electrode was mounted inside a luggin capillary to reduce the effects of IR drop.

The electrochemical behaviour of the electrode arrays was assessed by cyclic voltammetry recorded in 0.1 M KOH electrolyte at sweep rates of 5, 25 and 50 mV $s^{-1}$. The voltammetry was recorded in both de-oxygenated electrolyte (bubbled with Ar for 20 minutes prior to the measurements) and in oxygenated electrolyte (bubbled with $O_2$ for 20 minutes prior to the measurements).

## 3. Results and Discussion

### 3.1 Perovskite Characterisation

X-Ray diffraction of the STFO films, prepared at 650 °C under atomic oxygen, confirmed a cubic perovskite structure across the $SrTi_{1-x}Fe_xO_{3-y}$ tie-line (Supplementary Information S.2) consistent with expectation from bulk materials [16-18]. Figure 1A shows the intensity of the (110) reflection in a compositional gradient thin film in the region of this tie-line, and shows

the predominance of the cubic structure over a large range of compositions. The (110) peak intensity is the highest (reflecting more extensive crystallisation) for the Fe substituted perovskites. This is counterintuitive considering their higher formation energy as a result of a poorer fit of the Fe ion (in either of its oxidation state) in the perovskite B site when compared to titanium: This should make them more difficult to prepare thermodynamically. This is likely to reflect the effectiveness of the atomic co-evaporation method incorporating a plasma atom source which provides a low temperature route to oxygen stoichiometric oxides. Figure 1B shows that as the Fe content of the samples increases, there is a systematic shift in the $2\theta$ position of the (110) Bragg reflection due to the contraction of the crystal lattice caused by the replacement of $Ti^{4+}$ ions (r = 0.605 Å) with the smaller $Fe^{4+}$ ions (r = 0.585 Å). There is little change in the lattice with the Sr concentration. Indeed, there is a linear change in $2\theta$ with the concentration of Fe corresponding to a linear dependence of the lattice constant with B site substitution (Supplementary Information S3), i.e. the solid solution obeys Vegard's law between the two binary end members. What is striking about this result is that a range of bulk synthetic methodologies [17] [27] [28] [29] employing higher temperature conditions have not been successful in achieving such a solid solution chemistry of these cubic perovskite phases. We believe that this, again, reflects the advantages of the low temperature route to stoichiometric synthesis employed in this study.

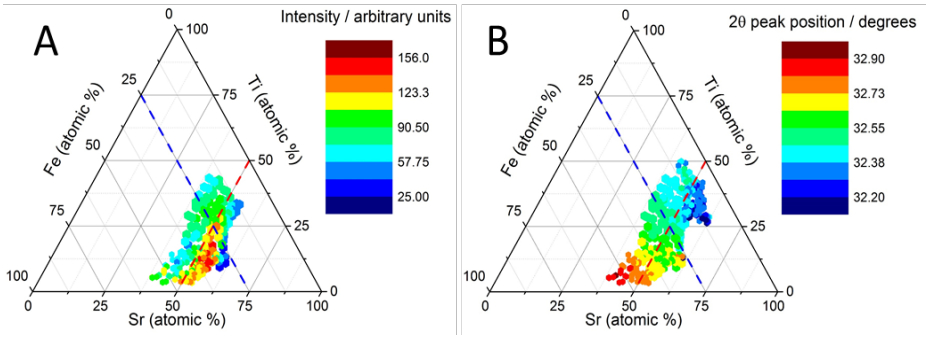


Figure 1 Ternary compositional plots showing (A) the variation in the intensity and (B) the $2\theta$ position of the cubic perovskite (110) Bragg reflection in XRD of thin films of $SrTi_{1-x}Fe_xO_{3-y}$. The peak intensity was correct to account for variations in film thickness as measured by profilometry which varied from 200 to 420 nm. Additional data is shown for the 2θ peak position from a sample deposited with low Ti content, this sample was however much thinner (ca. 100 nm) and intensity data could not be reliably obtained and corrected.

Despite the lack of evidence of a lattice distortion from the diffraction data, Raman measurements (Supplementary Information S4) of the STFO samples were not consistent with a cubic structure in which all lines should be disallowed by symmetry rules. An O-stretching vibrational mode was identified which had previously been observed in the

literature and assigned to a Jahn-Teller distortion which breaks they symmetry of the $BO_6$ octahedra by asymmetric relaxation of the B-O bonds [18].

The Jahn-Teller distortion is thought to arise due to the presence of a single $e_g$ electron in the electronic structure of the $Fe^{4+}$ ion which creates an un-equal charge distribution and is taken as evidence of the presence of the higher oxidation state. This theory does require the localisation of the $e_g$ electron which however should only be the case at low dopant concentrations since at a composition of x = 0.03 the electrons should be delocalised and form electronic bands [30]. Data taken from the $SrTi_{1-x}Fe_xO_{3-y}$ pseudo-binary line (Supplementary Information S4) showed that the line, which appeared at a wavenumber of 710 $cm^{-1}$ for compositions with low Fe content, decreased in intensity and moved to lower wavenumbers with increasing Fe content. This is consistent with a decreasing Jahn-Teller effect due to the delocalisation of the $e_g$ electron. However the observation of the O-stretching mode up to compositions as high as x = 0.8 suggests another cause and could be evidence of a cation or vacancy ordered superstructure which causes variation in the M-O bond lengths and disrupts the symmetry of the $MO_6$ octahedra.

The electrical conductivity of the STFO compositional gradient films, prepared at 650 °C under atomic oxygen, has been measured using Van-der Pauw 4-point probe in combination with the thickness measurement using profilometry. The variation in conductivity over a compositionally graded thin film samples is shown in Figure 2A. For compositions where x < 0.5, the conductivity was below the sensitivity of the instrument (ca. $1x10^{-6}$ S $cm^{-1}$). For compositions where x > 0.5 a monotonically increasing conductivity, consistent with expectations based on the literature [17, 31-33]. The dependence on Sr concentration is significantly lower. Figure 2B is a plot of the conductivity of the compositions close to the ideal perovskite phases $SrTi_{1-x}Fe_xO_{3-y}$ averaged along the tie line with Sr = 50 ± 5 at.% from (A). The conductivity of pure SFO is also included, and was measured on a uniform composition thin film of the perovskite.

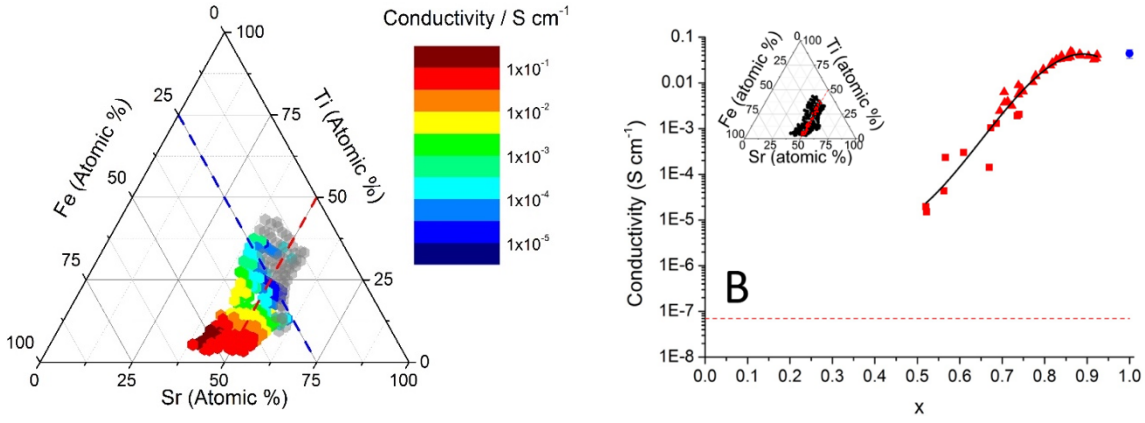

Figure 2 A) Ternary compositional plot of compositional gradient thin films in the region of the perovskites $SrTi_{1-x}Fe_xO_{3-y}$ of thickness ca. 300nm synthesized under atomic oxygen at 650 °C. The colours show the variation in the electrical conductivity measured by Van-der Pauw 4-point probe. Grey data points show compositions which exhibited sheet resistivity which were too large to be measured by the instrument. B) The conductivity of the compositions close to the ideal perovskite phases $SrTi_{1-x}Fe_xO_{3-y}$ averaged along the tie line with Sr = 50 ± 5 at.% from (A). The conductivity of pure SFO was measured on a uniform composition thin film of the perovskite.

The conductivity of pure SFO was 0.043 ± 0.01 S $cm^{-1}$ which is lower than values for bulk SFO which exceed 1 S $cm^{-1}$ [34]. This may be associated with oxygen deficiency in the thin film sample, since oxygen deficient SFO containing a proportion of $Fe^{3+}$ ions where electrons are localised are lower [35]. Indeed, comparison of our value for SFO to those of bulk samples [35] suggest that this oxygen deficiency may correspond to ca. y = 0.35. In the case of STFC perovskite composition (Figure 2B), the values that can be measured range from ca. 3 x $10^{-5}$ S $cm^{-1}$ for x = 0.5, exponentially increasing with Fe concentration to 0.041 S $cm^{-1}$ for x = 0.75 where it remains constant. In the region where conductivity could be measured, values are similar to bulk STFO materials prepared under an air atmosphere [32].

### 3.2 Redox Behaviour and Stability

Cyclic voltammetry recorded in deoxygenated 0.1 M KOH at sweep rates of 50, 25 and 5 mV $s^{-1}$ for a single electrode (of a 100-electrode array) of $SrTi_{0.5}Fe_{0.5}O_{3-y}$ deposited by PVD under atomic oxygen at 650 °C is shown in Figure 3. The voltammetry is dominated by two redox couples R1 (A1/C1) and R2 (A2/C2) around $0.8V_{RHE}$ and $1.4V_{RHE}$ respectively, and oxygen evolution above $1.5V_{RHE}$. The peak currents associated with R1 and R2 are both linearly proportional to the sweep rate, indicative of the redox process of a surface bound species. The peak separation and broadness of A2/C2 are suggestive of slow electron transfer kinetics.

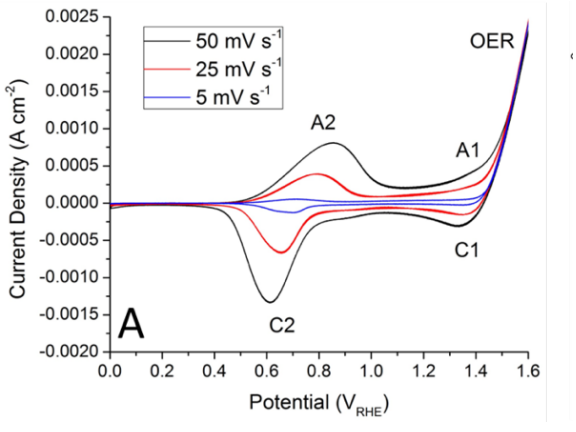

Figure 3 Cyclic voltammetry recorded in deoxygenated 0.1 M KOH at sweep rates of 50, 25 and 5 mV $s^{-1}$ on a thin film array electrode with composition $SrTi_{0.5}Fe_{0.5}O_{3-y}$ deposited by PVD at 650 °C under atomic oxygen. Data shown is the second cycle. The voltammetry is dominated by a redox couple A2/C2 for which the potential and peak current of the peaks vary with sweep rate.

The R1 redox couple has an equilibrium potential close to that reported (1.35 $V_{RHE}$) for the $Fe^{3+}/Fe^{4+}$ redox on mixed $Fe(OH)_2$ and $Ni/Fe(OH)_2$ films [36, 37]. The more dominant R2 redox couple is present at lower potential and we suggest this peak arises from the redox of Fe ions in the perovskite lattice which is able to stabilise the $Fe^{4+}$ oxidation state and as such lowers the equilibrium potential of the redox reaction. The R1 redox couple is therefore assumed to be associated with the $Fe^{3+}/Fe^{4+}$ redox of lower co-ordinated Fe ions in which the $Fe^{4+}$ oxidation state is less well stabilised by the lattice. For the two chemical environments, the surface process is:

$$Fe^{3+} - OH^{-}(s) + OH^{-}(aq) \rightleftharpoons Fe^{4+} - O^{2-}(s) + H_2O\,(aq) + e^{-} \qquad \text{Equation 1}$$

The redox reaction is not however limited to a surface process and previous studies [38] have confirmed that for perovskites able to support oxygen vacancies, such as $SrFeO_3$, oxide ions formed in this reaction can be intercalated into vacancy sites in the perovskite lattice by diffusion of $O^-$ which forms readily by charge transfer:

$$Fe^{4+}(s) + O^{2-}(s) \rightleftharpoons Fe^{3+}(s) + O^{-}(s) \qquad \text{Equation 2}$$

Since the redox reaction is not limited to the surface Fe sites and involves bulk Fe, the charge associated with this redox is expected to exceed that which would be expected for surface Fe sites alone: Indeed, this is observed experimentally.

The ternary plots in Figure 4 show the variation in charge under the oxidation peak (A2) and reduction peak (C2) from the cyclic voltammetry (Figure 3) recorded in deoxygenated 0.1 M KOH (sweep rate = 50 mV $s^{-1}$) on $SrTi_{1-x}Fe_xO_{3-y}$ model electrocatalyst thin films deposited by PVD at 650 °C under atomic oxygen. The $SrTi_{1-x}Fe_xO_{3-y}$ tie-line is shown by the dashed lines. The highest redox charge is observed at high Fe contents and at compositions lying close to the $SrTi_{1-x}Fe_xO_{3-y}$ tie-line, supporting the assignment of R2 to a $Fe^{3+}/Fe^{4+}$ redox couple in the perovskite structure.

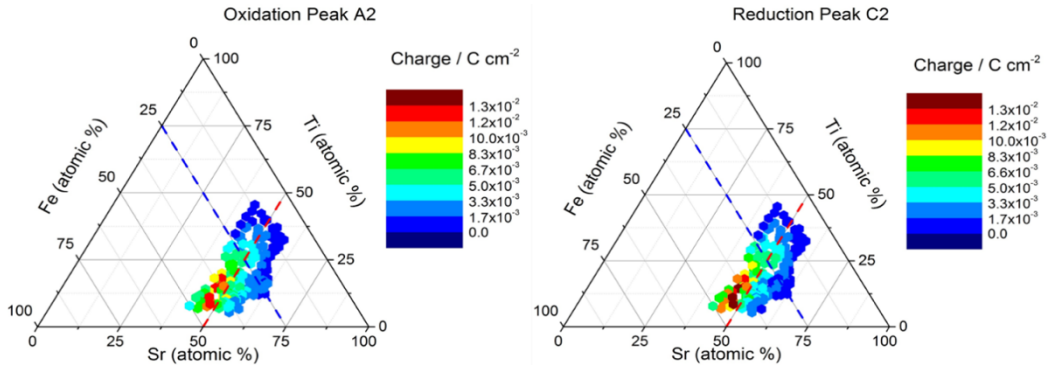


Figure 4 Ternary plot with colour map showing the variation in charge under the oxidation peak (A2) and reduction peak (C2) from the cyclic voltammetry (Figure 3) recorded in deoxygenated 0.1 M KOH with a sweep rate of 50 mV $s^{-1}$, on $SrTi_{1-x}Fe_xO_{3-y}$ model electrocatalysts in the form of thin films deposited by PVD at 650 °C under atomic oxygen. The $SrTi_{1-x}Fe_xO_{3-y}$ tie-line is shown by the dashed lines.

The number of moles of Fe involved in the R2 redox process has been calculated from the geometric charge density of C2, and compared to the number of moles of Fe expected in the surface. This charge corresponds (Supplementary Information S5) to an equivalent of between 20-30 monolayers for $SrTi_{1-x}Fe_xO_{3-y}$ where $x > 0.5$. This has assumed a roughness factor of 1, however even for a high roughness factor of 10 the result supports the supposition that the process involves a coupling of a surface redox (Equation 1) coupled to a bulk intercalation process (Equation 2).

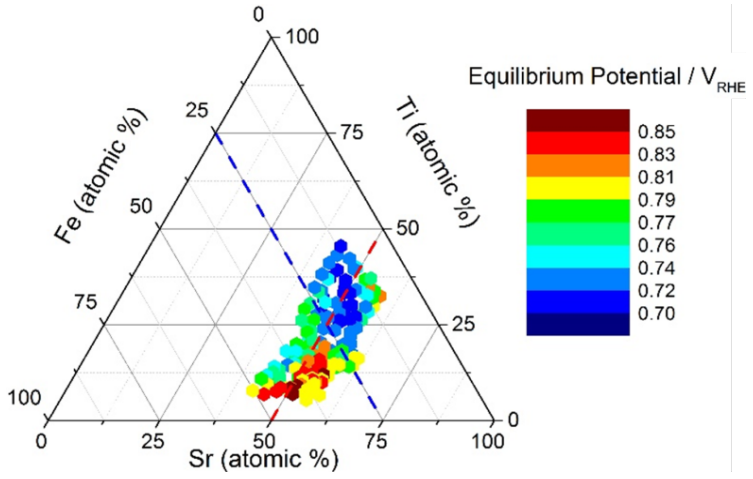


Figure 5 Ternary plot with colour map showing the variation in the equilibrium potential of the R2 redox, calculated from $E_{C2}$ + (($E_{A2}$-$E_{C2}$)/2). Data obtained from cyclic voltammetry, recorded in deoxygenated 0.1 M KOH, on $SrTi_{1-x}Fe_xO_{3-y}$ model electrocatalysts in the form of thin films deposited by PVD at 650 °C under atomic oxygen.

The equilibrium potential of a redox reaction reflects the ease of addition of an electron to the oxidised species or conversely the removal of an electron from the reduced species. A negative shift in the potential of the redox process corresponds to a stabilisation of the oxidised state whilst a positive shift represents stabilisation of the reduced state. The equilibrium potential of the the $Fe^{3+}/Fe^{4+}$ redox couple R2 in the region of the STFO compositional range as shown in Figure 5, and reveals an increase in the equilibrium potential with increasing Fe concentration along the perovskite tie-line. This is consistent with an increase in the electron density in the Fe(3d) states with an increasing Fe/Ti ratio: The Fe(3d) states form anti-bonding interactions with the O(2p) orbitals and so an increase in electron density would be expected to weaken the M-O bonding and stabilise the reduced state.

In order to investigate the stability of the perovskite electrocatalysts EDX measurements were taken on the samples before and after a series of the electrochemical experiments which included cycling between 0 $V_{RHE}$ and 1.6 $V_{RHE}$ at sweep rates of 5, 25 and 50 mV $s^{-1}$ in oxygenated and de-oxygenated 0.1 M KOH solution. This does not establish the total loss of material, but provides an indication of preferential loss of any element as a result of dissolution in the electrolyte. Figure 6A shows the compositions of 100 catalysts around the $SrTi_{1-x}Fe_xO_{3-y}$ tie-line obtained from EDX measurements prior to electrochemical cycling. A series of these catalysts along the tie-line are high-lighted by red points. EDX measurements following electrochemical cycling of the same 100 catalysts are shown in Figure 6B. Striking is that compositions with Sr content in excess of the $SrTi_{1-x}Fe_xO_{3-y}$ tie-line undergo a significant compositional change upon electrochemical cycling particularly corresponding and this is most notable at the highest Fe contents. The compositions close to the $SrTi_{1-x}Fe_xO_{3-y}$ tie-line, shown in red, appear quite stable although at the most Fe rich compositions there appears to be loss of Sr. These results are consistent with the trends in the equilibrium potential associated with the $Fe^{3+}/Fe^{4+}$ redox couple R2 (Figure 5). It should be noted that $SrTi_{1-x}Fe_xO_{3-y}$ perovskite catalysts prepared with molecular oxygen which are sub-stoichiometric in oxygen (not shown) are considerably less stable than the more oxygen stoichiometric catalysts prepared using the plasma atom source.

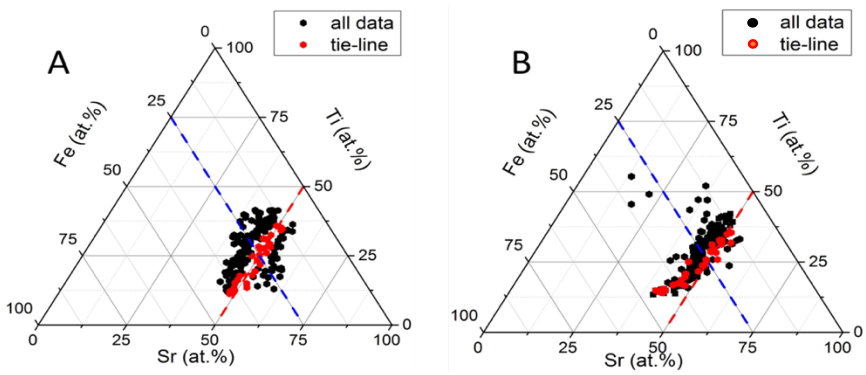


Figure 6 Ternary plots showing compositions obtained from SEM-EDX on 100 STFO catalysts prepared at 650 °C using an oxygen plasma before (A) and after (B) a series of electrochemical experiments, including cycling between 0 $V_{RHE}$ and 1.6 $V_{RHE}$. A series of points have been highlighted in red which sit along the tie line before electrochemical cycling so that their position after cycling is highlighted after cycling.

### 3.3 Oxygen Evolution and Oxygen Reduction Activity

Oxygen evolution (OER) activity was measured simultaneously on an array of 100 catalysts using cyclic voltammetry, recorded in deoxygenated 0.1 M KOH electrolyte at a sweep rate of 5 mV $s^{-1}$. This was carried out for compositions in the region of the $SrTi_{1-x}Fe_xO_{3-y}$ tie-line, synthesising the perovskites using an oxygen plasma. Some examples of the OER currents for selected compositions along the tie-line are shown in the Supplementary Information S6. Increasing the Fe content in the perovskite leads to an increase in the OER activity. This is summarised in Figure 7 which shows plots in ternary compositional space of the variation in the OER current density at 1.6 $V_{RHE}$, and the OER ignition potential at 100 μA for the 100 catalysts around the pseudo-binary tie line of $SrTi_{1-x}Fe_xO_{3-y}$. Oxygen evolution activity increases with both increasing Sr and Fe concentrations, as measured by both the current density and the ignition potential. While Sr rich compositions with respect to the tie-line exhibit OER activity, Sr poor compositions have lower activity. Compositions which are Sr rich with respect to the tie-line have been shown to be unstable (Figure 6) and hence it is the perovskites $SrTi_{1-x}Fe_xO_{3-y}$ which are of most interest.

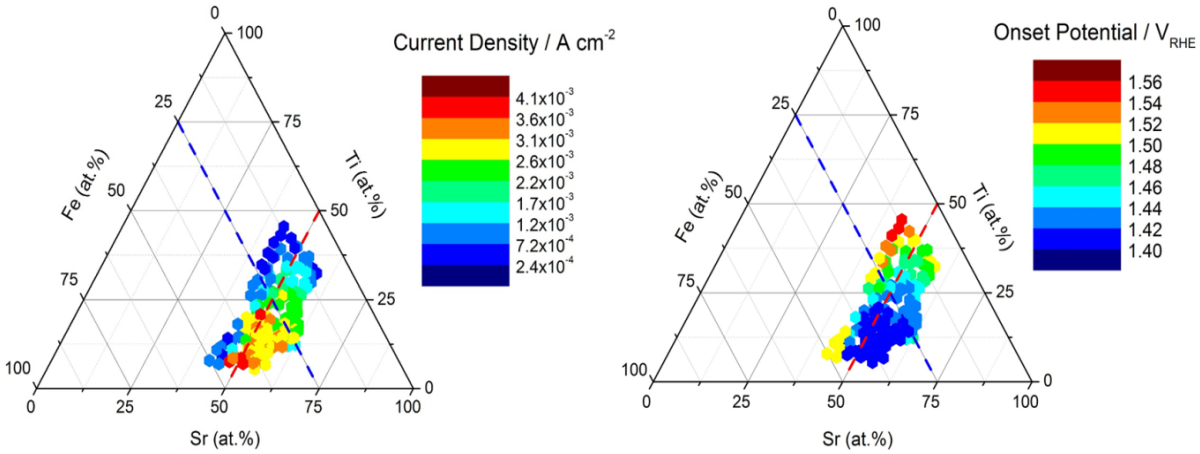


Figure 7 Ternary compositional plots around the perovskite $SrTi_{1-x}Fe_xO_{3-y}$ tie-line showing the OER activity measured in cyclic voltammetry (deoxygenated 0.1 M KOH at a sweep rate of 5 mV $s^{-1}$) simultaneously on 100 catalysts: A) current density at 1.6 $V_{RHE}$ and B) ignition potential at 100 µA. Examples of the cyclic voltammetry from which the data has been extracted are shown in the Supplementary Information S6.

There is a monotonic increase (Figure 7) in OER activity with increasing Fe concentration in $SrTi_{1-x}Fe_xO_{3-y}$. The onset (ignition) potential at 100 µA and the current density at 1.6 $V_{RHE}$ of the OER reaction for $SrTi_{1-x}Fe_xO_{3-y}$ as a function of x is shown in Figure 8A and Figure 8B respectively. The perovskite has been synthesised using the plasma atom source at a substrate temperature of 650ºC. The results have been extracted from the 100 catalyst measured in Figure 7 with a perovskite stoichiometry 50+/- 5 at% Sr. The onset potential decreases quickly for x < 0.5 and at higher Fe concentrations, the onset potential reduces more slowly. The current density shows a concomitant increase which is near linear up to x = 0.7, then shows a small decrease before increasing again at x = 7.5. We do not associate any apparent changes in catalytic activity (or redox behaviour) with the change in conductivity of the perovskites, despite the fact that the lower OER currents are observed on the more resistive oxides (Figure 2). There is no indication of an IR contribution in any of the electrochemical measurements, and the films are sufficiently thin to present a conductivity sufficient for the electrochemical measurements. The change in the trends is assumed to relate to a change in the mechanism from an adsorbate based mechanism at lower values of x to a mechanism involving participation of lattice oxygen. Previous studies [41] suggest that mechanisms involving participation of lattice oxygen offer higher activity but lower catalyst stability, this is consistent with the results of stability tests presented in Figure 6.

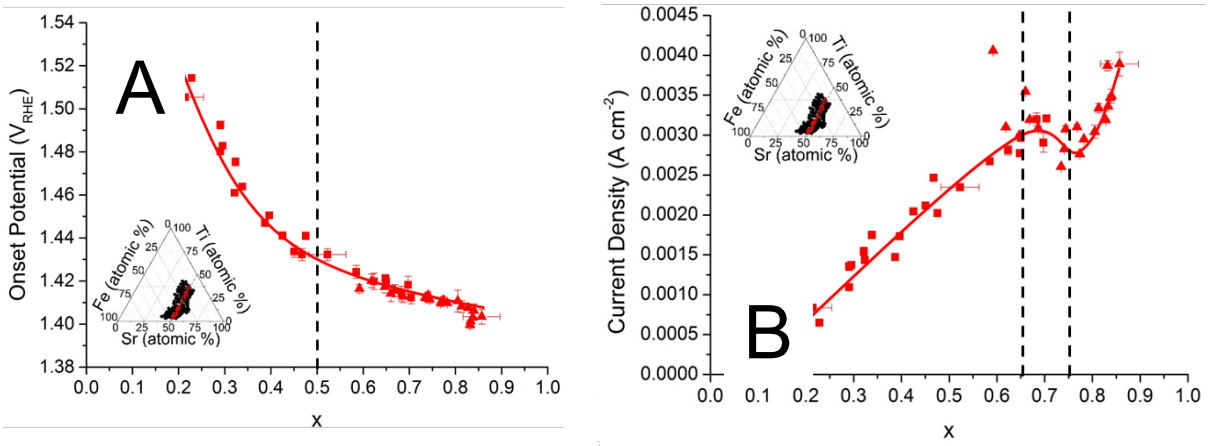


Figure 8 Variation in the onset (ignition) potential at 100 μA with varying Fe content, x, of $SrTi_{1-x}Fe_xO_{3-y}$ electrodes deposited by PVD at 650 °C under atomic oxygen. Variation in current density at 1.6 $V_{RHE}$ with varying Fe content, x, of $SrTi_{1-x}Fe_xO_{3-y}$ electrodes deposited by PVD at 650 °C under atomic oxygen.

Oxygen reduction on the $SrTi_{1-x}Fe_xO_{3-y}$ catalysts prepared at 650°C with an oxygen plasma (the most oxygen stoichiometric oxides) was characterised by a large overpotential for the reaction. Cyclic voltammetry for a $SrTi_{0.5}Fe_{0.5}O_{3-y}$ catalyst deposited under atomic oxygen is shown in Figure 9 restricting the maximum anodic potential to 1.2$V_{RHE}$ (1.15 $V_{RHE}$ initial potential, first scan positive) : The result is shown for measurement in de-oxygenated 0.1 M KOH (black) and oxygenated 0.1 M KOH (red). The cathodic scan in both cases is characterised by the reduction of the surface through C2 (Figure 3). In the case of the oxygenated electrolyte, this is accompanied by oxygen reduction below 0.3$V_{RHE}$. This is consistent with the model for oxygen reduction on a perovskite surface which is the displacement of the surface hydroxide on a reduced surface by oxygen [3]. This step is followed by the formation of surface peroxide. To show that the oxygen reduction observed at 0.3$V_{RHE}$ on oxygen stoichiometric $SrTi_{1-x}Fe_xO_{3-y}$ was associated with the rate determining peroxide $2e^-$ reduction step, experiments were carried out in deoxygenated 0.1 M KOH containing 5 mmol of hydrogen peroxide (not shown): A reduction wave identical to that shown for the ORR reaction in oxygenated electrolyte in Figure 9A was indeed observed.

In order to explore the sensitivity of the ORR reaction to the oxygen stoichiometry of the $SrTi_{1-x}Fe_xO_{3-y}$, similar experiments were carried out on catalysts prepared using molecular oxygen, rather than using a plasma of atomic oxygen. The oxides synthesised exhibit the perovskite structure, but the lower chemical potential during synthesis is likely to result in oxygen sub-stoichiometry. The results in Figure 9B show the cathodic scan in cyclic voltammetry in an oxygenated electrolyte, for a series of oxygen sub-stoichiometric

perovskite catalysts with varying Fe contents (x). The reduction associated with the R2 redox, C2, is much less prominent for all compositions than in the oxygen stoichiometric perovskite. Immediately following the oxide reduction in the cathodic scan, oxygen reduction is observed below 0.58$V_{RHE}$. A second oxygen reduction wave is also observed at 0.3$V_{RHE}$. This second wave of oxygen reduction is at the same potential as that observed on the oxygen stoichiometric perovskite (Figure 9A) and is therefore also likely to be associated with the 2$e^-$ reduction of the surface peroxide species. It is therefore tempting to speculate that the second oxygen reduction observed at the higher potential (the lower overpotential) is associated with a 4$e^-$ process, although this has not been confirmed experimentally. What is clear, however, is that an additional channel for oxygen reduction at lower overpotential has become available on the oxygen sub-stoichiometric oxides. The onset potential for the ORR reaction at 0.58$V_{RHE}$ on the oxygen sub-stoichiometric perovskites is found to reduce as x increases to x = 0.5 (Figure 9B), and is constant at higher concentrations of Fe in the lattice.

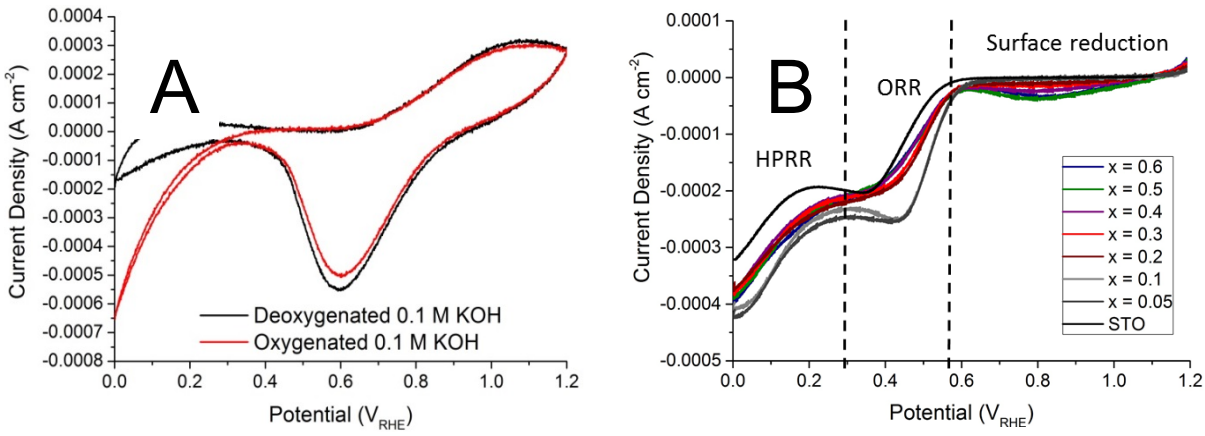


Figure 9 A) Cyclic voltammetry recorded in deoxygenated (black) and oxygenated (red) 0.1 M KOH at a sweep rate of 50 mV $s^{-1}$ for an electrode of composition $SrTi_{0.5}Fe_{0.5}O_{3-y}$ deposited by PVD at 650 °C under atomic oxygen. B) Cyclic voltammetry recorded in oxygenated 0.1 M KOH at a sweep rate of 5 mV $s^{-1}$ for oxygen sub-stoichiometric (synthesized with molecular oxygen) $SrTi_{1-x}Fe_xO_{3-y}$ catalyst compositions of varying x.

This is exemplified clearly in Figure 10, where the compositional dependence of the onset potential for ORR, defined for a current of 50 µA and extracted from slow scan voltammetry (Figure 9) on 100 electrocatalysts in a thin film $SrTi_{0.5}Fe_{0.5}O_{3-y}$ library is presented. The catalysts have been synthesized using molecular oxygen in order to produce oxygen sub-stoichiometry in the perovskites. The highest onset potential (i.e. the lowest overpotential for ORR) is observed for low concentrations of Fe (low values of x), and increasing the Fe

content to x = 0.3 decreases the onset potential which subsequently remains relatively constant in the range 0.3 < x < 0.7. There appears, therefore to be an anti-correlation between the activity for ORR (Figure 10) and OER (Figure 8) all be it on the oxygen sub-stoichiometric, and stoichiometric perovskites respectively.

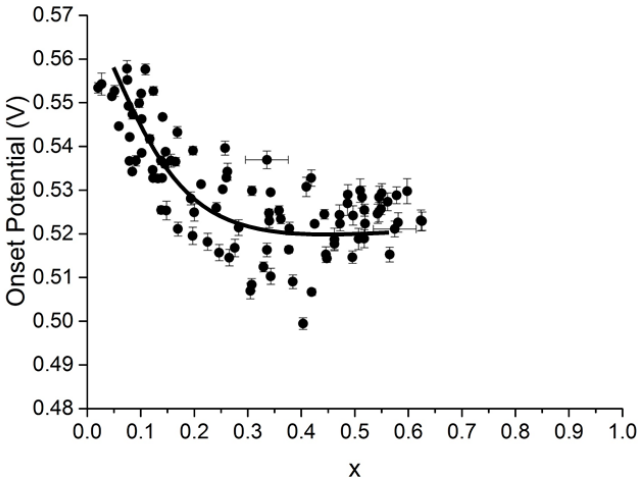


Figure 10 A plot showing variation in the onset potential ($V_{RHE}$) at 50 μA for the ORR with varying Fe content for a $SrTi_{1-x}Fe_xO_{3-y}$ thin film library synthesised with molecular oxygen.

## 4. Conclusions

Perovskite thin films with compositions $SrTi_{1-x}Fe_xO_{3-y}$ were successfully deposited by HT-PVD at 650 °C using a 500 W oxygen plasma. The use of this reactive oxygen source combined with atomic evaporation sources for deposition of the metallic elements allowed for intimate mixing of the elements and lowered the energy of formation of the crystalline perovskite material. They enabled the use of a lower temperature for synthesis than that required for traditional solid-state synthesis methods.

X-ray diffraction measurements confirmed a cubic perovskite structure for the thin films of composition $SrTi_{1-x}Fe_xO_{3-y}$ for all values of x. Lattice constant refinements confirmed a linear decrease in the lattice constant of the perovskite cell with increasing Fe content from 0.392 ± 0.001 nm for $SrTiO_3$ to 0.386 ± 0.001 nm for $SrFeO_3$. This is in accordance with Vergard's law for metallic alloys and provides evidence that the film constitutes a homogeneous solid solution with crystallites which contain both Fe and Ti cations. The presence of vibrational lines in the Raman spectra which would be disallowed by symmetry for the cubic perovskite structure suggests however that localised distortions from the cubic structures may occur. Conductivity measurements on the oxygen plasma-prepared thin film samples using the Van

der Pauw 4-point probe method showed an increase in conductivity with increasing Fe content consistent with previous studies [17, 31-33].

Cyclic voltammetry of the STFO films deposited onto electrode arrays revealed redox activity which was strongly correlated with the Fe content of the films and believed to correspond to the oxidation and reduction of Fe ions which occurs alongside the intercalation of oxygen into oxygen vacancy sites, as shown in Equation 3. Two distinct sets of redox peaks were identified and assigned to Fe in different chemical environments in the perovskite.

$$Fe^{3+} - V_{\ddot{O}} - Fe^{3+} + 2OH^- \rightleftharpoons Fe^{4+} - O - Fe^{4+} + H_2O + 4e^- \qquad \text{Equation 3}$$

The number of moles of Fe involved in the redox reaction was calculated from the Faradaic charge under the redox peaks and was found to greatly exceed the number of moles of Fe estimated to be present at the electrode surface. This is explained by the ability of the perovskite lattice to intercalate the surface oxygen into the bulk lattice by diffusion of oxygen to vacancy sites which frees up the surface ions to participate in further reaction. This process was found to be reversible with oxygen also being removed from the lattice upon reduction. This reversible electrochemical intercalation of oxygen has previously been observed for $SrFeO_{3-y}$ [38-40] but no literature studies on the electrochemical redox of the STFO material could be found.

The electrocatalytic activity of the STFO perovskites towards oxygen evolution was found to be tuneable with composition. High OER activity, characterised by over-potentials as low as 0.2 V, was found for compositions with x > 0.5 and close to or higher than stoichiometric Sr content (Sr ≥ 50 at.%). The high OER activity was however found to correlate with low stability of the electrodes towards electrochemical cycling. It is also proposed that the favourable activity in this region of compositional space arises from participation of lattice oxygen in the OER mechanism. The facile exchange of lattice oxygen may also be linked to the catalyst instability.

OER mechanisms involving lattice oxygen have been proposed as an alternative to the usual “adsorbate” mechanism in which all of the oxygen evolved originates from the solution [5, 41, 42]. The adoption of this mechanism relates to the ability of a catalyst to support oxygen vacancies and has been predicted for $SrFeO_{3-y}$ [42]. Whilst the adoption of the lattice oxygen mechanism results in high OER activity there is a clear link with poor electrode stability and so a balancing act between the two factors is required to identify a material with optimal properties for practical application in a fuel cell environment [5, 42]. For the STFO materials investigated in this work an optimal composition of $SrTi_{0.5}Fe_{0.5}O_{3-y}$ would be

recommended as the OER activity shows no significant increase with Fe content above this point whilst there is a significant decrease in the electrode stability.

The electrocatalytic activity of the STFO perovskites towards oxygen reduction was less impressive as the reaction did not occur on oxygen stoichiometric oxide surface. It is therefore assumed that for ORR electrocatalysis the reduced protonated surface must be accessible as the bonding in the $Fe^{4+}$-$O^{2-}$ is too strong for displacement by the oxygen molecule. This highlights the importance of considering the reaction surface when selecting candidates for electrocatalysis, and in particular the equilibrium potential of the redox reactions. It is interesting to note that ORR activity on the oxygen sub-stoichiometric perovskites showed the opposite trend with compositional variation to OER activity on the oxygen stoichiometric perovskites.

## 5. Acknowledgements

We would like to acknowledge the contribution of Jin Yeo who measured the thickness of the thin film electrocatalysts using the stylus profilometer.

## References

[1] Z.W. Chen, D. Higgins, A.P. Yu, L. Zhang, J.J. Zhang, A review on non-precious metal electrocatalysts for PEM fuel cells, Energ Environ Sci 4(9) (2011) 3167-3192.

[2] Y. Matsumoto, H. Manabe, E. Sato, Oxygen Evolution on La1-Xsrxcoo3 Electrodes in Alkaline-Solutions, J Electrochem Soc 127(4) (1980) 811-814.

[3] J. Suntivich, K.J. May, H.A. Gasteiger, J.B. Goodenough, Y. Shao-Horn, A Perovskite Oxide Optimized for Oxygen Evolution Catalysis from Molecular Orbital Principles, Science 334(6061) (2011) 1383-1385.

[4] J.O. Bockris, T. Otagawa, The Electrocatalysis of Oxygen Evolution on Perovskites, J Electrochem Soc 131(2) (1984) 290-302.

[5] A. Grimaud, K.J. May, C.E. Carlton, Y.L. Lee, M. Risch, W.T. Hong, J.G. Zhou, S.H. Yang, Double perovskites as a family of highly active catalysts for oxygen evolution in alkaline solution, Nat Commun 4 (2013).

[6] E. Rios, J.L. Gautier, G. Poillerat, P. Chartier, Mixed valency spinel oxides of transition metals and electrocatalysis: case of the MnxCo3-xO4 system, Electrochim Acta 44(8-9) (1998) 1491-1497.

[7] N. Li, X.M. Yan, W.J. Zhang, B.X. Lin, Electrocatalytic activity of spinel-type oxides LiMn2-XCoXO4 with large specific surface areas for metal-air battery, J Power Sources 74(2) (1998) 255-258.

[8] U.F. Vogt, P. Holtappels, J. Sfeir, J. Richter, S. Duval, D. Wiedenmann, A. Zuttel, Influence of A-Site Variation and B-Site Substitution on the Physical Properties of (La,Sr)FeO3 Based Perovskites, Fuel Cells 9(6) (2009) 899-906.

[9] A. Wattiaux, J.C. Grenier, M. Pouchard, P. Hagenmuller, Electrolytic Oxygen Evolution in Alkaline-Medium on La1-Xsrxfeo3-Y Perovskite-Related Ferrites .2. Influence of Bulk Properties, J Electrochem Soc 134(7) (1987) 1718-1724.

[10] C.Z. Yuan, H.B. Wu, Y. Xie, X.W. Lou, Mixed Transition-Metal Oxides: Design, Synthesis, and Energy-Related Applications, Angew Chem Int Edit 53(6) (2014) 1488-1504.

[11] Y.L. Cao, H.X. Yang, X.P. Ai, L.F. Xiao, The mechanism of oxygen reduction on MnO2-catalyzed air cathode in alkaline solution, J Electroanal Chem 557 (2003) 127-134.

[12] F.H.B. Lima, M.L. Calegaro, E.A. Ticianelli, Investigations of the catalytic properties of manganese oxides for the oxygen reduction reaction in alkaline media, J Electroanal Chem 590(2) (2006) 152-160.

[13] I.A. Raj, K.I. Vasu, Characterization of Electrolytic Mno2-Based Oxygen Electrodes for Alkaline Water Electrolyzer Fuel-Cell Reactions, Int J Hydrogen Energ 15(10) (1990) 751-756.

[14] I. Roche, E. Chainet, M. Chatenet, J. Vondrak, Carbon-supported manganese oxide nanoparticles as electrocatalysts for the Oxygen Reduction Reaction (ORR) in alkaline medium: Physical characterizations and ORR mechanism, J Phys Chem C 111(3) (2007) 1434-1443.

[15] M. Cardona, Optical Properties and Band Structure of SrTiO3 and BaTiO3, Physical Review 140(2A) (1965) A651-A655.

[16] P. Adler, S. Eriksson, Structural properties, Mossbauer spectra, and magnetism of perovskite-type oxides SrFe1-xTixO3-y, Z Anorg Allg Chem 626(1) (2000) 118-124.

[17] S. Steinsvik, R. Bugge, J. Gjonnes, J. Tafto, T. Norby, The defect structure of SrTi1-xFexO3-y (x=0-0.8) investigated by electrical conductivity measurements and electron energy loss spectroscopy (EELS), J Phys Chem Solids 58(6) (1997) 969-976.

[18] M. Vracar, A. Kuzmin, R. Merkle, J. Purans, E.A. Kotomin, J. Maier, O. Mathon, Jahn-Teller distortion around Fe(4+) in Sr(Fe(x)Ti(1-x))O(3-delta) from x-ray absorption spectroscopy, x-ray diffraction, and vibrational spectroscopy, Phys Rev B 76(17) (2007).

[19] J. Suntivich, H.A. Gasteiger, N. Yabuuchi, H. Nakanishi, J.B. Goodenough, Y. Shao-Horn, Design principles for oxygen-reduction activity on perovskite oxide catalysts for fuel cells and metal-air batteries (vol 3, pg 546, 2011), Nat Chem 3(8) (2011) 647-647.

[20] S. Guerin, B.E. Hayden, Physical vapor deposition method for the high-throughput synthesis of solid-state material libraries, J Comb Chem 8(1) (2006) 66-73.

[21] P.S. Anderson, S. Guerin, B.E. Hayden, M.A. Khan, A.J. Bell, Y. Han, M. Pasha, K.R. Whittle, I.M. Reaney, Synthesis of the ferroelectric solid solution, Pb(Zr1-xTix)O-3 on a single substrate using a modified molecular beam epitaxy technique, Appl Phys Lett 90(20) (2007).

[22] M.S.B. Darby, S. Guerin, B.E. Hayden, H.J. Schreiner, S. Yakovlev, High throughput physical vapour deposition and dielectric and ferroelectric screening of (Bi,Na)TiO3 thin-film libraries, J Appl Phys 113(1) (2013).

[23] S. Canulescu, T. Lippert, A. Wokaun, R. Robert, D. Logvinovich, A. Weidenkaff, M. Dobeli, M. Schneider, Preparation of epitaxial La0.6Ca0.4Mn1-xFexO3 (x=0, 0.2) thin films: Variation of the oxygen content, Prog Solid State Ch 35(2-4) (2007) 241-248.

[24] M.S.B. Darby, D.V. Karpinsky, J. Pokorny, S. Guerin, A.L. Kholkin, S. Miao, B.E. Hayden, I.M. Reaney, Synthesis and characterization of Bi-1 (-) xNdxFeO3 thin films deposited using a high throughput physical vapour deposition technique, Thin Solid Films 531 (2013) 56-60.

[25] S. Guerin, B.E. Hayden, C.E. Lee, C. Mormiche, A.E. Russell, High-throughput synthesis and screening of ternary metal alloys for electrocatalysis, J Phys Chem B 110(29) (2006) 14355-14362.

[26] S. Guerin, B.E. Hayden, C.E. Lee, C. Mormiche, J.R. Owen, A.E. Russell, B. Theobald, D. Thompsett, Combinatorial electrochemical screening of fuel cell electrocatalysts, J Comb Chem 6(1) (2004) 149-158.

[27] F. Schulze-Küppers, S.F.P. ten Donkelaar, S. Baumann, P. Prigorodov, Y.J. Sohn, H.J.M. Bouwmeester, W.A. Meulenberg, O. Guillon, Structural and functional properties of SrTi1−xFexO3−δ ($0 \leqslant x \leqslant 1$) for the use as oxygen transport membrane, Separation and Purification Technology 147 (2015) 414-421.

[28] M. Ghaffari, M. Shannon, H. Hui, O.K. Tan, A. Irannejad, Preparation, surface state and band structure studies of SrTi(1 (-) x)Fe(x)O(3 (-) (delta)) (x=0-1) perovskite-type nano structure by X-ray and ultraviolet photoelectron spectroscopy, Surf Sci 606(5-6) (2012) 670-677.

[29] L.F. da Silva, M.I.B. Bernardi, L.J.Q. Maia, G.J.M. Frigo, V.R. Mastelaro, Synthesis and thermal decomposition of SrTi1-x Fe (x) O-3 (0.0 a parts per thousand currency sign x a parts per thousand currency sign 0.1) powders obtained by the polymeric precursor method, J Therm Anal Calorim 97(1) (2009) 173-177.

[30] R. Evarestov, E. Blokhin, D. Gryaznov, E.A. Kotomin, R. Merkle, J. Maier, Jahn-Teller effect in the phonon properties of defective SrTiO3 from first principles, Phys Rev B 85(17) (2012).

[31] L.H. Brixner, Preparation and properties of the SrTi1−xFexO3−x2/Ox2 system, Mater Res Bull 3(4) (1968) 299-308.

[32] L.F. da Silva, J.C. M'Peko, J. Andres, A. Beltran, L. Gracia, M.I.B. Bernardi, A. Mesquita, E. Antonelli, M.L. Moreira, V.R. Mastelaro, Insight into the Effects of Fe Addition on the Local Structure and Electronic Properties of SrTiO3, J Phys Chem C 118(9) (2014) 4930-4940.

[33] A. Rothschild, W. Menesklou, H.L. Tuller, E. Ivers-Tiffee, Electronic structure, defect chemistry, and transport properties of SrTi1-xFexO3-y solid solutions, Chem Mater 18(16) (2006) 3651-3659.

[34] J.B. Torrance, P. Lacorro, C. Asavaroengchai, R.M. Metzger, Simple and Perovskite Oxides of Transition-Metals - Why Some Are Metallic, While Most Are Insulating, J Solid State Chem 90(1) (1991) 168-172.

[35] Y. Takeda, R. Kanno, T. Kondo, O. Yamamoto, H. Taguchi, M. Shimada, M. Koizumi, Properties of Srmo3-Delta (M=Fe,Co) as Oxygen Electrodes in Alkaline-Solution, J Appl Electrochem 12(3) (1982) 275-280.

[36] X.H. Li, F.C. Walsh, D. Pletcher, Nickel based electrocatalysts for oxygen evolution in high current density, alkaline water electrolysers, Phys Chem Chem Phys 13(3) (2011) 1162-1167.

[37] J.Y.C. Chen, L.N. Dang, H.F. Liang, W.L. Bi, J.B. Gerken, S. Jin, E.E. Alp, S.S. Stahl, Operando Analysis of NiFe and Fe Oxyhydroxide Electrocatalysts for Water Oxidation: Detection of Fe4+ by Mossbauer Spectroscopy, J Am Chem Soc 137(48) (2015) 15090-15093.

[38] A. Wattiaux, L. Fournes, A. Demourgues, N. Bernaben, J.C. Grenier, M. Pouchard, A Novel Preparation Method of the Srfeo3 Cubic Perovskite by Electrochemical Means, Solid State Commun 77(7) (1991) 489-493.

[39] A. Nemudry, P. Rudolf, R. Schollhorn, Topotactic electrochemical redox reactions of the defect perovskite SrCoO2.5+x, Chem Mater 8(9) (1996) 2232-2238.

[40] A. Piovano, G. Agostini, A.I. Frenkel, T. Bertier, C. Prestipino, M. Ceretti, W. Paulus, C. Lamberti, Time Resolved in Situ XAFS Study of the Electrochemical Oxygen Intercalation in SrFeO2.5 Brownmillerite Structure: Comparison with the Homologous SrCoO2.5 System, J Phys Chem C 115(4) (2011) 1311-1322.

[41] W.G. Hardin, J.T. Mefford, D.A. Slanac, B.B. Patel, X.Q. Wang, S. Dai, X. Zhao, R.S. Ruoff, K.P. Johnston, K.J. Stevenson, Tuning the Electrocatalytic Activity of Perovskites through Active Site Variation and Support Interactions, Chem Mater 26(11) (2014) 3368-3376.

[42] X. Rong, J. Parolin, A.M. Kolpak, A Fundamental Relationship between Reaction Mechanism and Stability in Metal Oxide Catalysts for Oxygen Evolution, Acs Catal 6(2) (2016) 1153-1158.